

Bayesian reconstruction of memories stored in neural networks from their connectivity

Sebastian Goldt^{*1}, Florent Krzakala², Lenka Zdeborová³ and Nicolas Brunel^{4,5}

¹International School of Advanced Studies (SISSA), Trieste, Italy

²IdePHICS laboratory, École Fédérale Polytechnique de Lausanne (EPFL), Switzerland

³SPOCS laboratory, École Fédérale Polytechnique de Lausanne (EPFL), Switzerland

⁴Department of Neurobiology, Duke University, Durham, NC, USA

⁵Department of Physics, Duke University, Durham, NC, USA

18th May 2021

Abstract

The advent of comprehensive synaptic wiring diagrams of large neural circuits has created the field of connectomics and given rise to a number of open research questions. One such question is whether it is possible to reconstruct the information stored in a recurrent network of neurons, given its synaptic connectivity matrix. Here, we address this question by determining when solving such an inference problem is theoretically possible in specific attractor network models and by providing a practical algorithm to do so. The algorithm builds on ideas from statistical physics to perform approximate Bayesian inference and is amenable to exact analysis. We study its performance on three different models and explore the limitations of reconstructing stored patterns from synaptic connectivity.

Introduction

Comprehensive synaptic wiring diagrams or “connectomes” provide a detailed map of all the neurons and their interconnections in a brain region or even an entire organism. Since the connectome of the nematode *C. elegans* was obtained using electron microscopy methods in 1986 [1], methods for data acquisition and analysis have both been scaled up and improved significantly. Today, it has become possible to provide connectomes of much more complex systems such as various *Drosophila melanogaster* circuits [2, 3], or even a large part of its brain [4, 5]; the olfactory bulb of zebrafish [6]; and various pieces of the rodent retina [7–9], hippocampus [10], and cortex [11–14]. While there still remain a number of formidable challenges on the way to the complete connectome of a mammal or even human brain [15], the data sets available today already give rise to a number of intriguing questions. At the same time, it is becoming increasingly clear that new quantitative methods must be developed to fully exploit the new troves of data that connectomics provides [16].

Here, we focus on local neural networks that store information in their synaptic connectivity. It has been hypothesised that cortical networks with their extensive recurrent synaptic connectivity are optimised for this task [17]. A popular model for these networks are attractor neural networks such as the Hopfield’s model [18] and various generalisations [19–22], where memories are stored as

^{*}sebastian.goldt@sissa.it

attractor states of the dynamics. These attractor states represent learned internal representations of external stimuli that have been presented repeatedly to the network during training, inducing changes in synaptic weights of the network. One natural question to ask is then: given the knowledge of the synaptic connections between neurons in a recurrent neural network, can we reconstruct the patterns of activity that were stored in this network in the first place?

In this paper, we first give a mathematical formulation of this problem in terms of a Bayesian inference problem. This approach has the advantages of providing a natural way to handle the uncertainty associated with estimating a large number of parameters from a large number of noisy observations, *i.e.* the reconstruction of the original stimuli from the strength of the synapses in the networks in the present case. We then use tools from statistical physics to both determine when solving this inference problem is theoretically possible in a model setting, and to provide a practical algorithm to do so. We analyse the performance of the algorithm in detail on a variety of different problems, and we invite the reader to download our reference implementation of the algorithm on [GitHub](#) and to use and extend it.

The task: Reconstructing memories from recurrent neural networks

We analyse a variant of the celebrated Hopfield model [18] for a recurrent neural network composed of N interacting neurons with state s_i , $i = 1, \dots, N$. The network is fully-connected with symmetric, bidirectional connections that have a scalar weight $J_{ij} = J_{ji} \in \mathbb{R}$. The neurons update their state at time $t + 1$ sequentially according to $s_i^{t+1} = g(a_i^t)$, where $g(\cdot)$ is some non-linear activation function and $a_i^t = \sum_{j \neq i} J_{ij} s_j^t$ is the total synaptic input of the i th neuron.

The network stores P fixed patterns or memories, which are N -dimensional vectors that we collect in the matrix $\mathbf{X}^* \in \mathcal{X}^{P \times N}$. We write $\mathbf{X}_{\mu,:}^*$ for the μ th pattern stored in the network, and \mathcal{X} denotes the set of values that pattern entries can take, *e.g.* $\mathcal{X} = \{\pm 1\}$ for binary patterns. Patterns are stored in the network by choosing its weights J_{ij} such that the patterns $\mathbf{X}_{\mu,:}^*$ become fixed points of its dynamics. We will study this model in the thermodynamic limit $N \rightarrow \infty$, while keeping the number of patterns P of order 1.

A classic idea for choosing the weights $\mathbf{J} = [J_{ij}] \in \mathbb{R}^{N \times N}$ is to make the weights proportional to the empirical correlation of the patterns, $W_{ij} \sim \sum_{\mu} X_{\mu,i}^* X_{\mu,j}^*$. This prescription is also known as the Hebb rule [23] and can be written more compactly as

$$\mathbf{J} = \mathbf{W} = \frac{1}{\sqrt{N}} \mathbf{X}^* (\mathbf{X}^*)^\top, \quad (1)$$

where $(\mathbf{X}^*)^\top$ is the transpose of \mathbf{X}^* and \mathbf{W} is thus the empirical correlation matrix of the patterns. With binary neurons $s_i(t) = \pm 1$, this model corresponds to the celebrated Hopfield model [18]. In this model, the network exhibits fixed point attractors close to the stored memories, provided the number of stored patterns P is smaller than $\alpha_c N$ where $\alpha_c \sim 0.14$ [24].

The model described by Eq. (1) has a number of unrealistic features that makes it inadequate for the problem we are interested in here: (i) The network is fully connected, at odds with neuronal networks in the brain; (ii) Synapses are not sign-constrained, while synapses in the brain are either excitatory (*i.e.* non-negative) or inhibitory (*i.e.* non-positive). A minimal model that satisfies both requirements is the *rectified Hopfield model*

$$J_{ij} = \Phi(W_{ij} - \tau + \zeta_{ij}) \geq 0 \quad (2)$$

where $\Phi(x) = \max(0, x)$ which ensures that weights are non-negative, ζ_{ij} is a noise term (see below), and the scalar parameter τ controls the connection probability in the network,

$$p_C = \frac{1}{2} \operatorname{erfc} \left(\frac{\tau}{\sqrt{2}\nu} \right) \quad (3)$$

to leading order as $N \rightarrow \infty$. In particular, the network becomes sparse in the large τ limit. Since $P \sim O(1)$, the weights obtained from Eq. 1 will have variance $1/N$, while the noise has variance of order 1.

The noise matrix ζ_{ij} is taken to be a symmetric random Gaussian matrix, i.e. for $i < j$, ζ_{ij} s are i.i.d. random Gaussian variables with mean zero and standard deviation $\nu \sim \mathcal{O}(1)$, and $\zeta_{ji} = \zeta_{ij}$. In brain networks, connectivity matrices are not symmetric. However, if we assume that the weights depend on the stimuli only via the symmetric matrix $\mathbf{X}^*(\mathbf{X}^*)^\top$, these asymmetries will be due to the different sources of noise in the formation of the network and the measurement of the synaptic weights. Without loss of generality, we can hence symmetrise the matrix \mathbf{J} , or equivalently focus on the case where the noise matrix ζ_{ij} is symmetric.

The model we study is related to a family of connectivity matrices studied by Sompolinsky [25], and bears similarities with a model recently proposed by [26]. Note that our model is effectively a model of a network of excitatory neurons. This is consistent with the hypothesis that information storage occurs primarily in excitatory-to-excitatory synapses, while the job of inhibitory neurons is primarily to control the level of activity in the excitatory network. This view is consistent with a number of studies [27, 28] but has been challenged by others [26]. We will come back to this issue in the Discussion.

We emphasise that our focus in this paper is the *reconstruction* of stimuli from an observed connectivity matrix \mathbf{J} . Our choice choice of scaling in Eq. (1) can then be motivated via random matrix theory [29]: We have a random matrix ζ_{ij} with elements drawn i.i.d. from the normal distribution with variance $\nu \sim \mathcal{O}(1)$. By adding a low-rank perturbation $W = \mathbf{X}\mathbf{X}^\top/\sqrt{N}$, where the entries of \mathbf{X} are $\mathcal{O}(1)$, we put ourselves in the regime where reconstruction of the $\mathcal{O}(N)$ entries of \mathbf{X} from the $\mathcal{O}(N^2)$ observations we obtain via the connectivity matrix is possible for some choices of ν and τ , while other scalings would result in problems that are either trivial or impossible to solve for any combination of (ν, τ) . Reconstruction is *not* the retrieval problem, where we ask whether the patterns \mathbf{X} are stable fixed points of the dynamics of the Hopfield network [18, 30–32]. The retrieval problem has a rich history, in particular in statistical physics, but it will not be our focus here.

Solving the inference problem using statistical physics

Our aim is to reconstruct the patterns \mathbf{X}^* that were used to create the connectivity matrix \mathbf{J} of a Hopfield network using the learning rule (2). We will call the patterns \mathbf{X}^* the ground truth of the problem. Since the learning rule is stochastic, we formulate the pattern reconstruction as a probabilistic inference problem: given a noisy observation \mathbf{J} of the symmetric low-rank matrix $\mathbf{W} \sim \mathbf{X}\mathbf{X}^\top$ through a noisy output channel corresponding to the learning rule (2), what is \mathbf{X} ? The output channel corresponding to the learning rule (2) is characterised by the conditional probability distribution

$$P_{\text{out}}(J_{ij} = 0 | W_{ij}) = \frac{1}{2} \operatorname{erfc} \left(\frac{W_{ij} - \tau}{\sqrt{2}\nu} \right), \quad (4a)$$

$$P_{\text{out}}(J_{ij} | W_{ij}) = \frac{\exp \left(-(J_{ij} - W_{ij} + \tau)^2 / 2\nu^2 \right)}{\sqrt{2\pi}\nu} \quad \text{for } J_{ij} > 0. \quad (4b)$$

Reconstructing low-rank matrices from noisy observations is a generic inference problem that appears in a lot of different applications, such as robust [33] and sparse [34–36] PCA, Gaussian mixture clustering [37], and community detection in dense networks [38, 39], to name but a few.

In the following, we will assume that we know the hyper-parameters ν and τ that were used to generate the connectivity matrix \mathbf{J} , but note that expectation maximisation and related techniques seem like a natural candidate to extend our approach to cases where we would need to learn these

hyper-parameters. We will further assume that we know the *a priori* distribution $P_{\mathbf{X}}(\mathbf{X})$ over patterns that were stored in the network, and that this distribution is factorized as $P_{\mathbf{X}}(\mathbf{X}) = \prod_i^N P_X(\mathbf{x}_i)$. This distribution could for example reflect the fact that we know that the memories stored in the network are binary, encoding whether a given neuron is firing or not, and that we have an idea of the probability that any given neuron is firing in a given memory. Adopting a Bayesian approach [40] to the inference of the pattern matrix \mathbf{X} given the connectivity \mathbf{J} , we use Bayes' theorem to write down the so-called posterior distribution over patterns given the connectivity matrix as:

$$P(\mathbf{X}|\mathbf{J}) = \frac{1}{Z(\mathbf{J})} \prod_i^N P_X(\mathbf{x}_i) \prod_{j>i}^N P_{\text{out}}(J_{ij}|X_{ij}) \quad (5)$$

where we introduced the shorthand $\mathbf{x}_i = \mathbf{X}_{:,i}$ for the i th column of \mathbf{X} . The marginals $p(\mathbf{x}_i)$ of this distribution, obtained by integrating out all \mathbf{x}_j , $j \neq i$, provide the best estimate of the patterns that can be performed [40]. However, evaluating this high-dimensional integral exactly is an intractable problem. Instead, here we exploit the formal analogy between the posterior distribution (5) and certain probability distributions that arise in statistical physics to derive an algorithm called “approximate message passing” [41], which performs approximate Bayesian inference of the memories stored in the network. Furthermore, we will demonstrate that techniques from statistical physics, in particular a tool called “state evolution” (SE), can be used to analyse the behaviour and the performance of this algorithm in quite some detail. Approximate message passing algorithms can be understood as a variant of belief propagation, a general algorithm for inference in graphical models that is usually credited to Pearl [42].

Results

A Bayesian algorithm for pattern reconstruction

The inference problem considered here, where we aim to recover a symmetric low-rank matrix from noisy observations, can be solved using a class of approximate message passing (AMP) algorithms for low-rank matrix factorisation called Low-RAMP. It was derived by Lesieur et al. [43], building on previous works [35, 44, 45] that provided AMP algorithms for particular instances of low-rank matrix factorisation problems. Low-RAMP is an iterative algorithm that produces estimates for the mean $\hat{\mathbf{x}}_i$ of the marginal distribution $p(\mathbf{x}_i)$ and their covariance matrix σ_i . Using this framework, we will derive variants of the algorithm for the pattern reconstruction problem outlined in the previous section. We present the algorithm in detail in the Methods section.

We also provide a [reference implementation](#), a reference implementation of Low-RAMP for symmetric and bipartite matrix factorisation problems applicable to a number of different problems. It is designed to be easily extendable to other problems and also provides a number of further convenience methods. All the results in this paper can be reproduced using this code.

State evolution

Low-RAMP algorithm has the distinctive advantage over other algorithms, such as Monte Carlo methods, that its behaviour in the limit $N \rightarrow \infty$ for separable prior on the \mathbf{X}^* , random i.i.d. noise ξ_{ij} , and number of patterns $P = O(1)$, can be tracked exactly and at all times using the “state evolution” technique [41, 46]. The roots of this method go back to ideas originally introduced in physics to deal with a class of disordered systems called glasses [47, 48]. For the low-rank matrix factorisation problems we consider here, state evolution was derived and analysed in detail by Lesieur et al. [43], building on previous works that derived and analysed state evolution for other specific problems [35, 36, 44]. The last few

years in particular have seen a surge of interest in using state evolution to understand the properties of approximate Bayesian inference algorithms for a number of problems [49].

Our goal is to track the mean-squared error mse_X of the reconstruction \hat{x}_i^t of the true signal \mathbf{x}_i^* after t steps,

$$\text{mse}(t) \equiv \frac{1}{N} \sum_i^N \|\hat{x}_i^t - \mathbf{x}_i^*\|_2^2, \quad (6)$$

where $\|\cdot\|_2^2$ denotes the Euclidean norm of a vector. The mse can be expressed in terms of a single matrix-valued parameter defined as

$$\mathbf{M}^t \equiv \frac{1}{N} \sum_i^N \hat{x}_i^t \mathbf{x}_i^{*,\top} \in \mathbb{R}^{P \times P}, \quad (7)$$

such that $\text{mse}(t) = \text{Tr} [\langle \mathbf{x}_0 \mathbf{x}_0^\top \rangle - \mathbf{M}^t]$. Here and throughout this paper we write averages with respect to the prior distribution $p_X(\mathbf{x})$ of the corresponding model as $\langle \cdot \rangle$.

Now the goal is to find an update equation for the order parameter M^t that mirrors the progress of the algorithm. This update equation is the state evolution equation [41, 46]. Remarkably, from [50] we see that the two constants defining our problem, τ and ν , do not appear explicitly in the state evolution equations. Instead, the behaviour of the algorithm – and hence its performance – only depends on an effective signal-to-noise ratio (SNR) of the problem, which is a function of the threshold τ and noise variance ν utilised in the learning rule (2). Formally, it can be expressed as the inverse of the Fisher information [51] of the generative model we use to describe how the network is connected (4a)-(4b), evaluated at $W_{ij} = \mathbf{x}_i \mathbf{x}_j^\top / \sqrt{N} = 0$:

$$\frac{1}{\Delta} \equiv \mathbb{E}_{P_{\text{out}}(J|w=0)} \left(\frac{\partial \ln P_{\text{out}}(J|w)}{\partial w} \right)_{J,w=0}^2 \quad (8)$$

$$= \frac{\tau e^{-\tau^2/2\nu^2}}{\sqrt{2\pi\nu^3}} + \frac{e^{-\tau^2/\nu^2}}{\pi\nu^2 \text{erfc}(-\tau/\sqrt{2\nu})} + \frac{1}{2\nu^2} \text{erfc}\left(\frac{\tau}{\sqrt{2\nu}}\right). \quad (9)$$

In fact, on the level of the algorithm, everything about the output channel (4) can be summarised in this single, scalar quantity Δ . This remarkable universality of the state evolution and hence the AMP algorithm with respect to the output channel was first observed in [50] and dubbed “channel universality”.

State evolution provides an update equation for the order parameter M^t that mirrors the progress of the algorithm. In all the cases considered in this paper, it reads [43]

$$\mathbf{M}^{t+1} = \mathbb{E}_{\mathbf{x}_0, \mathbf{w}} \left[f_{\text{in}} \left(\frac{\mathbf{M}^t}{\Delta}, \frac{\mathbf{M}^t}{\Delta} \mathbf{x}_0 + \sqrt{\frac{\mathbf{M}^t}{\Delta}} \mathbf{w} \right) \mathbf{x}_0^\top \right] \quad (10)$$

where \mathbf{w} is a P -dimensional vector of Gaussian random variables with mean zero and variance 1. The average over \mathbf{x}_0 is taken with respect to the prior distribution $p_X(\mathbf{x})$. The function f_{in} depends on the prior over stored patterns and the output channel as

$$f_{\text{in}}(\mathbf{A}, \mathbf{b}) = \frac{1}{Z(\mathbf{A}, \mathbf{b})} \sum_{\mathbf{x} \in \mathcal{X}^P} \mathbf{x} p_X(\mathbf{x}) \exp \left(\mathbf{b} \mathbf{x} - \frac{1}{2} \mathbf{x}^\top \mathbf{A} \mathbf{x} \right). \quad (11)$$

where $Z(\mathbf{A}, \mathbf{b}) = \sum_{\mathbf{x} \in \mathcal{X}^P} p_X(\mathbf{x}) \exp(\mathbf{b} \mathbf{x} - 1/2 \mathbf{x}^\top \mathbf{A} \mathbf{x})$ is the normalisation factor, while $\mathbf{A} \in \mathbb{R}^{P \times P}$ and $\mathbf{b} \in \mathbb{R}^P$.

So to summarise, statistical physics gives us an algorithm to perform approximate inference of the patterns and the state evolution equation (10) allows us to track the behaviour of the algorithm over

time. We can thus analyse the performance of the algorithm in high-dimensional inference by studying the fixed points of the low-dimensional state-evolution (10). This is the key idea behind this approach, and we will now demonstrate the usefulness of this machinery by applying it to several specific cases.

Reconstructing binary patterns

As a first application of the algorithm and the analysis tools outlined so far, we consider the reconstruction of a set of binary patterns, $\mathcal{X} = \{\pm 1\}$. We will assume that both positive and negative values are equiprobable and that the components of a pattern vector are independent of each other, so the prior on a column of the matrix of stored patterns, \mathbf{x}_i , is simply

$$p_X(\mathbf{x}_i) = \prod_j^r p_x(x_{ij}) = \frac{1}{2^r}. \quad (12)$$

A single pattern ($P = 1$)

It is instructive and helpful for the following discussions to first consider the case where $P = 1$, *i.e.* there is only a single pattern stored in the network that we are trying to recover from \mathbf{J} . The threshold function for the model then becomes $f_{\text{in}}(A, B) = \tanh(B)$, with $B \in \mathbb{R}$, and the state evolution for the now scalar parameter m^t simplifies to

$$m^{t+1} = \int Dw \tanh \left(\frac{m^t}{\Delta} + \sqrt{\frac{m^t}{\Delta}} w \right) \quad (13)$$

where we have introduced a shorthand for the Gaussian measure $Dw \equiv e^{-w^2/2} / \sqrt{2\pi} dw$.

We can now iterate the state evolution equation (13) with a given noise level $\Delta(\nu, \tau)$ until convergence and then compute the mse corresponding to that fixed point. The fixed point we converge to reveals information about the performance of the AMP algorithm. We plot the results on the left-hand side of Fig. 1 for two different *initialisations* of the algorithm.

In blue, we plot the mse obtained by iterating SE starting with an *random initialisation*

$$m^{t=0} = 0 + \delta, \quad (14)$$

where $\delta > 0$ is a very small random number. The error obtained in this way is the one that is obtained by the AMP algorithm when initialised with a random draw from the prior distribution – in other words, a random guess for the patterns. This is confirmed by the blue crosses, which show the mean and standard deviation of the mse obtained from five independent runs of the algorithm on actual instances of the problem. The dashed orange line in Fig. 1 shows the final mse obtained from an informed initialisation

$$m^{t=0} = 1 - \delta, \quad (15)$$

which would correspond to initialising the algorithm with the solution, *i.e.* $\hat{x}_i = \mathbf{x}_i^*$.

In this model, we find that the AMP algorithm starting from a random guess performs just as well as the algorithm starting from the informed initialisation. This need not always be the case, and we will indeed find a different behaviour in the next sparse and skewed models we consider.

When is recovery possible? We can see from the right-hand plot of Fig. 1 that recovery of the memories from the connectivity \mathbf{J} is not always possible; for $\Delta > \Delta_c$, the mean-squared error of the solution obtained by the algorithm is indeed trivial, in the sense that we would have obtained the same mean-squared error had we made a random guess for the solution based on the prior distribution (12)

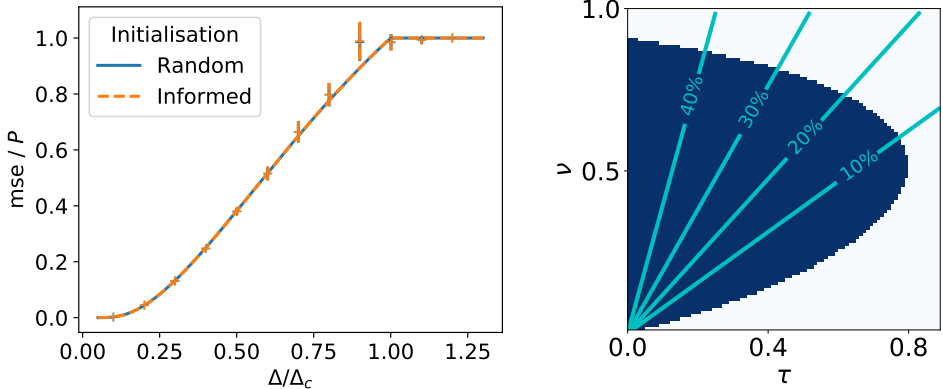


Figure 1: **(Left) Reconstruction and performance of the message-passing algorithm for binary patterns.** We plot the mse per pattern obtained by the AMP algorithm, Eq. (34), as a function of the effective noise Δ (8). We plot the performance of the algorithm starting from the random (14) and informed (15) initialisations. Lines depict the result of the state evolution, while crosses denote the performance of the AMP algorithm on an instance of the problem. Having $\Delta/\Delta_c > 1$ corresponds to the white region in the phase diagram on the right. In this model, AMP achieves the same performance regardless of initialisation. *Parameters:* $N = 5000, \tau = 0$. **(Right) Phase diagram for the rectified Hopfield channel with $P = 1$.** We plot whether reconstruction of the patterns better than a random guess is easy (blue) or impossible (white) using the message-passing algorithm as a function of the constant threshold τ and the variance of the Gaussian noise in the learning rule ν (2). The solid lines are the contours of the connection probability $p_C(\nu, \tau)$ (3).

alone. We can calculate this critical noise level Δ_c using the state evolution (10). We can see from that equation that $m^t = 0$ is a trivial fixed point, in the sense that the mse corresponding to that fixed point is equal to the mse obtained by making a random guess. Expanding Eq. (13) around this fixed point yields $m^{t+1} = m^t/\Delta$. There are hence two regimes for recovery, separated by a critical value

$$\Delta_c = 1 \quad (16)$$

of the effective noise (8). If $\Delta > \Delta_c$, the uniform fixed point is stable and recovery is impossible. On the other hand, for $\Delta < \Delta_c$, the uniform fixed point is unstable and hence Low-RAMP returns an estimate for the patterns that has an mse that is lower than random guessing. Fig. 1 shows the phase diagram delineating the easy and the impossible phase for the rectified Hopfield channel with symmetric prior (12).

At first sight, the impact of the additive Gaussian noise ζ_{ij} on the phase diagram in Fig. 1 appears counter-intuitive. If we fix the threshold to, say, $\tau = 0.5$, reconstruction is impossible for small variances ν of ζ_{ij} . As we increase ν , i.e. as we add *more* noise to the system, recovery becomes possible. The key to understanding this behaviour is that for a single stimulus $P = 1$, a weight in the network will have one of two possible values which are symmetric around the origin, $w_{ij} = \pm a$. By applying the rectification, for any cut-off $\tau > a$ the resulting weight matrix without additive noise is trivially zero and no recovery possible. We can only hope to detect something when adding ζ_{ij} pushes the value of the weight before rectification above the cut-off. Recovery then becomes possible if the added noise is large enough that the weight without noise is larger than the cut-off $a + \zeta_{ij} > \tau$, while remaining small enough that it's significantly more likely that the noise-less weight is positive than negative. As the noise variance increases even further, its detrimental effects dominate, and recovery becomes impossible again.

Another way to look at this phenomenon is to plot the critical variance of ζ_{ij} at which reconstruction becomes possible, ν^* , as a function of the connection probability p_C (3). We obtained this plot by solving, for a given value $p_C = c$, the two-dimensional system

$$\Delta = 1 \quad (17)$$

$$p_C = c \quad (18)$$

for (τ, ν) . We show the resulting plot in Fig. 2. As expected, the critical variance increases with the connection probability, and that it goes to zero as the connection probability goes to zero.

Many patterns ($P > 1$)

For the general case of several patterns $P > 1$ with finite P , we can significantly simplify the state evolution by noticing that the matrix M^t will interpolate between a matrix full of zeros at time $t = 0$ and a suitably scaled identity matrix in the case of perfect recovery, *i.e.* $M^t = a^t \mathbf{I}_P / \Delta$, where \mathbf{I}_P is the identity matrix in P dimensions. The threshold function becomes

$$[f_{\text{in}}(A, B)_k] = \tanh \left(\frac{a^t}{\Delta} x_{0,k} + \sqrt{\frac{a^t}{\Delta}} w_k \right) \quad (19)$$

Substituting into the state evolution gives an update equation for the parameter a^t , namely

$$a^{t+1} = \int D w_k \tanh \left(\frac{a^t}{\Delta} + \sqrt{\frac{a^t}{\Delta}} w_k \right) \quad (20)$$

which has the same form as the state evolution in the $P = 1$ case, Eq. (13). So we find, remarkably, that recovering P distinct patterns is exactly equivalent to recovering a single pattern P times. While this is true in thermodynamic limit $N \rightarrow \infty$ when we keep the number of patterns of order $P \sim \mathcal{O}(1)$, this approximation will eventually break down in practical applications with finite network sizes. We will investigate this further below.

Sparse patterns

An interesting variation of the rectified Hopfield model is its sparse version, where only a fraction $0 \leq \rho \leq 1$ of the components x_{ij} of a pattern \mathbf{x}_i are non-zero. The prior distribution then becomes

$$p_X(\mathbf{x}_i) = \prod_{j=1}^r p_x(x_{ij}) = \prod_{j=1}^r \left[(1 - \rho) \delta(x_{ij}) + \frac{\rho}{2} [\delta(x_{ij} - 1) + \delta(x_{ij} + 1)] \right], \quad (21)$$

where $\delta(\cdot)$ is the Kronecker delta. This prior has mean $\langle x \rangle = 0_p$, where 0_p is a vector of p zeros, and covariance $\langle xx^\top \rangle = \rho \mathbf{I}_p$. The state evolution will interpolate between an order parameter that is all zeros for an estimator that is drawn from the prior distribution and completely uncorrelated with

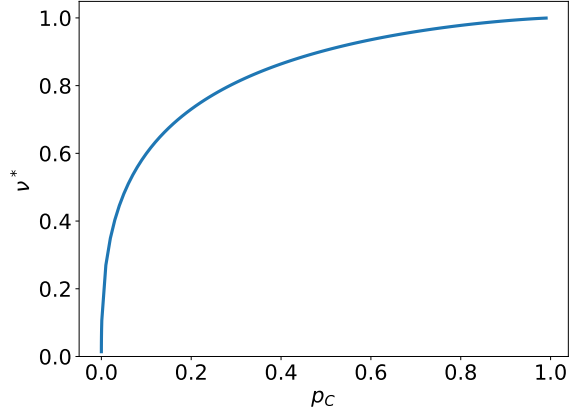


Figure 2: **Critical noise ν^* as a function of connection probability p_C .** We plot ν^* , the largest variance of the additive Gaussian noise ζ_{ij} at which reconstruction remains possible, against the probability p_C (3) that any two neurons are connected.

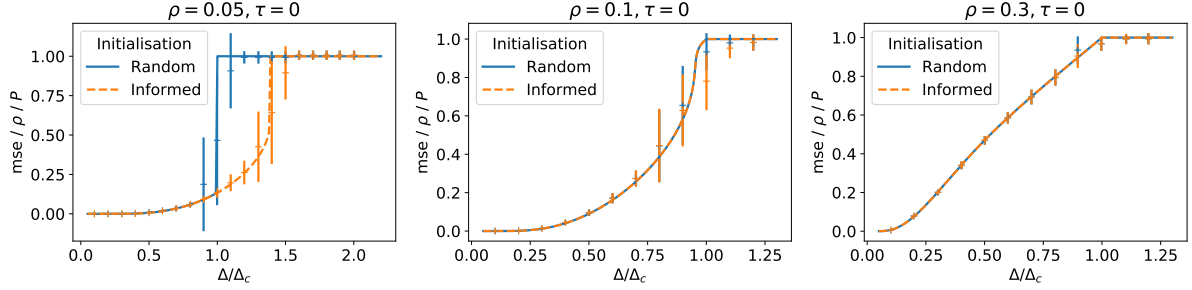


Figure 3: **Reconstructing sparse, binary patterns using message passing.** We plot the mse per pattern obtained by the AMP algorithm, Eq. (34), as a function of the effective noise Δ (8), for random (14) and informed (15) initialisations. Lines depict the result of the state evolution, while crosses denote the performance of the AMP algorithm on an instance of the problem. While AMP performs the same starting from both initialisations for $\rho = 0.1$ and $\rho = 0.3$, there is a gap in performance for $\rho = 0.05$, which might hint at the existence of a hard phase (see main text). *Parameters:* $N = 2000, \tau = 0$.

the ground truth, and $M = \rho \mathbf{I}_P$ for perfect reconstruction. We are thus motivated to use the ansatz $M^t = a^t \mathbf{I}_P$. The threshold function then becomes

$$[f_{\text{in}}(A, B)_k] = \frac{\rho e^{-A_{kk}/2} \sinh(B_k)}{1 + \rho [e^{-A_{kk}/2} \cosh(B_k) - 1]} \quad (22)$$

Substituting this form into the SE update equation (10) yields a closed update equation for the parameter a^t ,

$$a^{t+1} = \mathbb{E}_w \frac{\rho^2 e^{-a^t/2\Delta} \sinh(a^t/\Delta + \sqrt{a^t/\Delta} w)}{1 + \rho [e^{-a^t/2\Delta} \cosh(a^t/\Delta + \sqrt{a^t/\Delta} w) - 1]}, \quad (23)$$

where w is a scalar Gaussian random variable with zero mean and unity variance. We can recover the state evolution for the symmetric rectified Hopfield model from Eq. (23), in the limit $\rho \rightarrow 1$.

We plot the performance of Low-RAMP for the reconstruction of sparse patterns together with the theoretical predictions obtained using state evolution in Fig. 3 for different levels of sparsity. For $\rho = 0.1$ and $\rho = 0.3$ (middle and right plot, resp.), the plots resemble the results obtained for the symmetric Hopfield model: Reconstruction is possible if the effective noise level is below the critical noise level $\Delta_c = \rho^2$, which can again be obtained by linearising the state evolution equation (23) around its trivial fixed point $a^t = 0$. For these two values of the sparsity, the mse of the estimate returned by Low-RAMP (blue dashed line) matches the mse obtained starting from the informed initialisation. However, the two quantities disagree for smaller sparsity $\rho = 0.05$, (left), where there is range of effective noise levels Δ for which the performance of Low-RAMP does not match the Bayes-optimal prediction, which has a lower error. We note that this could be the signature of a computational-to-statistical gap, or *hard phase*, where a better-than-chance reconstruction is possible, but message-passing algorithms do not achieve it (see Refs. [49, 52] for recent reviews on the topic with many examples).

Reconstructing skewed patterns

As a third and final example, we consider the reconstruction of skewed patterns. For this, we will draw patterns from the prior distribution

$$p_X(\mathbf{x}_i) = \prod_{j=1}^r p_x(x_{ij}) = \prod_{j=1}^r [(1 - \rho)\delta(x_{ij} + \rho) + \rho\delta(x_{ij} - (1 - \rho))] \quad (24)$$

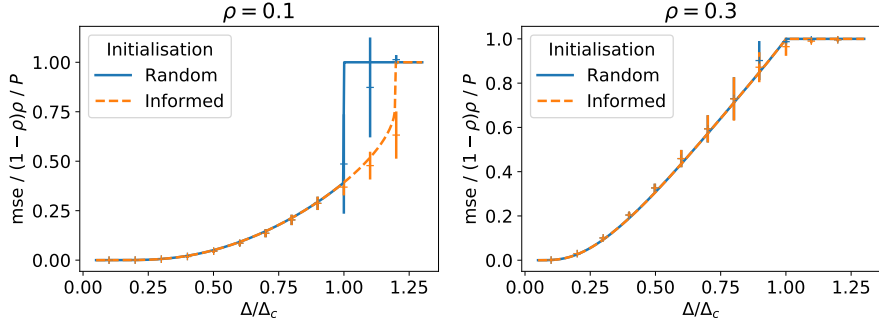


Figure 4: **Performance of the algorithm for stored patterns with Tsodyks' prior.** Same plot as Figures 1 and 3, for stored patterns drawn from Tsodyks' prior (24). For $\rho < 0.211$, the performance of the algorithm with random initialisation (14) is different from the performance with informed initialisation (15), which might be the signature of a hard phase. *Parameters:* $N = 2000, \tau = 0$.

which is related to models proposed first by Tsodyks and Feigel'man [19, 53]. This model has mean zero and a covariance matrix $\rho(1 - \rho)\mathbf{I}_P$. We still use the channel corresponding to the learning rule of the rectified Hopfield model (2), so while the Fisher information stays the same, we have a new threshold function (11) which reads

$$[f_{\text{in}}(A, B)_k] = 1 - \rho - \frac{1 - \rho}{1 - \rho (1 - e^{A_{kk}(\rho - 1/2) + B_k})} \quad (25)$$

The prior distribution (24) allows us to use the same ansatz for the magnetisation that we used previously. Setting $M^t = a^t \mathbf{I}_P$, we get the following update equation for the scalar order parameter $a^t > 0$:

$$a^{t+1} = \mathbb{E}_W \frac{(\rho - 1)^2 \rho^2 (e^{a^t/\Delta} - 1) e^{w\sqrt{a^t/\Delta}}}{\left(\rho e^{w\sqrt{a^t/\Delta}} - (\rho - 1)e^{a^t/2\Delta}\right) \left(\rho \exp\left(\frac{2w\sqrt{\Delta a^t} + a^t}{2\Delta}\right) - \rho + 1\right)}. \quad (26)$$

We plot the performance of the algorithm together with the results of iterating the state evolution equation for two different values of the skew parameter ρ in Fig. 4.

The hardness of recovering skewed patterns In this model too, we have a uniform fixed point with $a^t = 0$. Expanding around this fixed point yields the update equation

$$a^{t+1} = \frac{(\rho - 1)^2 \rho^2}{\Delta} a^t \quad (27)$$

so we find that the critical value of the noise where the uniform or uninformative fixed point becomes unstable in this model is $\Delta < \Delta_c = (\rho - 1)^2 \rho^2$.

Recently, a closed-form sufficient criterion for the existence of a hard phase in models that have a prior with zero mean was derived in [43]; namely, a hard phase exists if

$$\langle x^3 \rangle^2 > 2 \langle x^2 \rangle^3 \quad (28)$$

where the average is taken with respect to the prior distribution of this model, Eq. (21). For the prior (24), the criterion (28) predicts the existence of a first order phase transition and hence of a hard phase for $\rho > \rho_c = 1/2 - 1/\sqrt{12} \simeq 0.2113$ where we assume w.l.o.g. that $\rho < 1/2$. Note that this is a sufficient condition, and not a necessary one; in fact, it is not fulfilled for the sparse Hopfield prior, so we cannot calculate the critical value of ρ at which the hard phase appears in this way.

Reconstructing even more patterns: how far can we go?

A natural question that arises for the algorithms we have derived is how many patterns we can reliably reconstruct. In practice, the bottleneck for reconstructing the patterns is computing the exact threshold function f_{in} (11). For the simple Hopfield prior that we first discussed (12), computing the average in Eq. (11) requires the summing of 2^P terms so the computational cost is exponential in the number of patterns stored. We can circumvent this bottleneck by computing this function using a mean-field approximation [54], which was originally proposed in [55].

The mean-field approximation One of the difficulties that arise as we increase the number of patterns stored in the weights of the network is that it becomes non-trivial to evaluate the partition function of the Gaussian approximation of the posterior density of a column-vector \mathbf{x} (see the detailed explanation of the AMP algorithm in the Methods section):

$$W(\mathbf{x}; \mathbf{A}, \mathbf{b}) = \frac{1}{Z(\mathbf{A}, \mathbf{b})} p_X(\mathbf{x}) \exp \left(\sum_j^r b_j x_j - \frac{1}{2} \sum_{j,k}^r x_j A_{jk} x_k \right). \quad (29)$$

Since we have to evaluate the mean and the variance of this distribution at every step of the algorithm, it becomes essential to find a computationally feasible approximation for these quantities.

This is indeed possible by performing a mean-field approximation of (29) [54], which was originally proposed in [55]. We thus approximate the posterior distribution by a factorised distribution, replacing the full covariance matrix \mathbf{A} with a vector \mathbf{a} that contains only the variance of the $j = 1, \dots, P$ elements of \mathbf{x} ,

$$\tilde{W}(\mathbf{x}; \tilde{\mathbf{a}}, \tilde{\mathbf{b}}) = \prod_j^r \frac{1}{\tilde{Z}(\tilde{a}_j, \tilde{b}_j)} p_X(x_j) \exp \left(\tilde{b}_j x_j - \frac{1}{2} \tilde{a}_j x_j^2 \right). \quad (30)$$

where we use the tilde to denote mean-field quantities.

We have implemented mean-field approximations for the models discussed thus far and we show the performance of AMP with this approximation for the three models discussed so far in Fig. 5 together with the state evolution prediction for the reconstruction of a single stored pattern $P = 1$ without the mean-field approximation. The picture that emerges is similar for all three models studied here: the algorithm with the mean-field approximation is able to reconstruct the stored patterns just as well as if it was looking at the reconstruction of a single pattern up to a certain noise level, beyond which performance quickly deteriorates. Intuitively, the cross-talk between the stored patterns introduces an additional source of noise for the reconstruction, which leads to failure to reconstruct the stored patterns at lower Δ than in the case $P = 1$.

Scaling of the critical number of stored patterns Throughout this paper, we have relied on the assumption that the matrix \mathbf{J} is of low rank in all our derivations. The mean-field approximation that we just introduced makes it now computationally feasible to run the reconstruction algorithm even with a large number of patterns. This raises an important practical question: for which number of patterns does the algorithm based on the low-rank approximation break down?

We investigate this question in all three models numerically as follows. We fixed the noise level Δ in all experiments at 20% of the critical noise level beyond which it is information-theoretically impossible to weakly reconstruct the stored patterns. We then set the threshold for the reconstruction mse below which we consider the algorithm successful at 20% of the trivial mse obtained by random guessing. Going back to the example of storing P binary patterns, the mse $/P$ obtained by randomly guessing the components of each pattern is 1, so the threshold error for this model is 0.2, which we indicate by

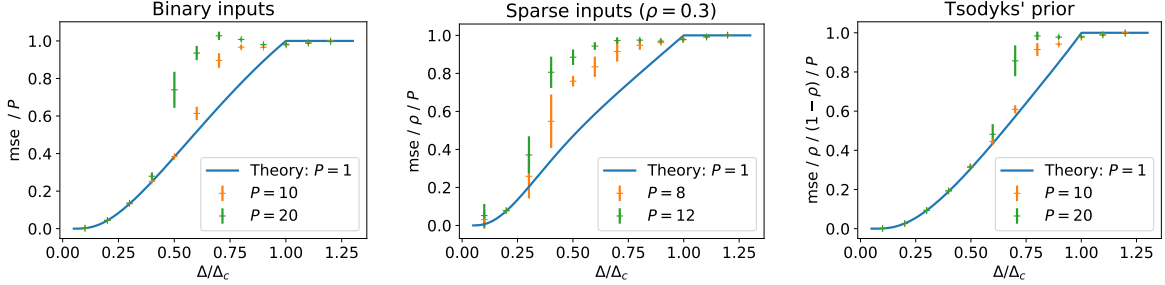


Figure 5: **MSE from reconstructing with the mean-field prior approximation.** We plot the final mse obtained by the AMP algorithm (no damping), using a mean-field approximation to compute the threshold function. The solid line is the mse predicted by iterating the state evolution for the scalar variable, Eq. (13). We choose $N = 5000$ and set $\tau = 0$.

the orange line on the left of Fig. 6. We then ran twenty reconstruction experiments with $N = 1000$ for each value of P , and each dot in the plot indicates the final mse for one experiment. We see that for $P = 25$, all twenty runs gave an mse well below the threshold; in fact, the reconstruction error per pattern mse / P is as low as if we had stored only a single pattern in the network (blue line). As we increase the number of patterns P , the first time the algorithm is not able to recover all patterns is for $P = 29$ patterns. At $P = 34$, the algorithm fails to achieve an mse below the threshold in more than 50% of the cases. We define the critical number of stored patterns P_{crit} as the largest number of patterns that can be reconstructed with an mse below the threshold in at least 50% of the runs, so $P_{\text{crit}} = 33$ in this case. On the right, we show the values of P_{crit} for all three models (binary, sparse and skewed) as a function of N . In each case, we find that $P_{\text{crit}} \sim N^\gamma$, with the exponent γ between $\gamma \approx 0.5$ for sparse patterns and $\gamma \approx 0.7$ for skewed patterns.

Discussion

We have derived the conditions under which it is possible to reconstruct the patterns stored in a recurrent Hopfield network from knowledge of the connections alone and have provided a practical algorithm to do so. In particular, we have studied the reconstruction of P patterns using the exact prior information, where P is of order 1, while we let the number of neurons in the network tend to infinity, $N \rightarrow \infty$. We have also explored a mean-field approximation of the prior that allowed us to study how the maximum number of patterns that can be reconstructed with some reliability scales with the pattern dimension. We now discuss some directions in which our work can be extended.

The case of unknown generative model We have assumed that the hyper-parameters of the problem, such as the number of stored stimuli P or the generative model of the stimuli $p_X(x)$, are known before reconstruction. However, it is possible to extend both the message-passing algorithm and its analysis to the case of unknown hyper-parameters. Within our framework, a natural approach to learn the values of these hyper-parameters is closely related to the well-known expectation maximisation algorithm [56]. A detailed study of expectation maximisation to obtain various hyper-parameters for message-passings algorithm was reported by Krzakala et al. [57] for the statistical estimation problem of “compressed sensing”, where one aims to reconstruct a signal from a number of measurements that is smaller than the number of unknowns. Another approach to deal with an unknown noise distribution was recently proposed by Montanari et al. [58] for the related problem of matrix denoising, where one aims to reconstruct an unknown, low-rank matrix $\mathbf{X} \in \mathbb{R}^{m \times n}$ from observations $\mathbf{Y} = \mathbf{X} + \mathbf{W}$ when

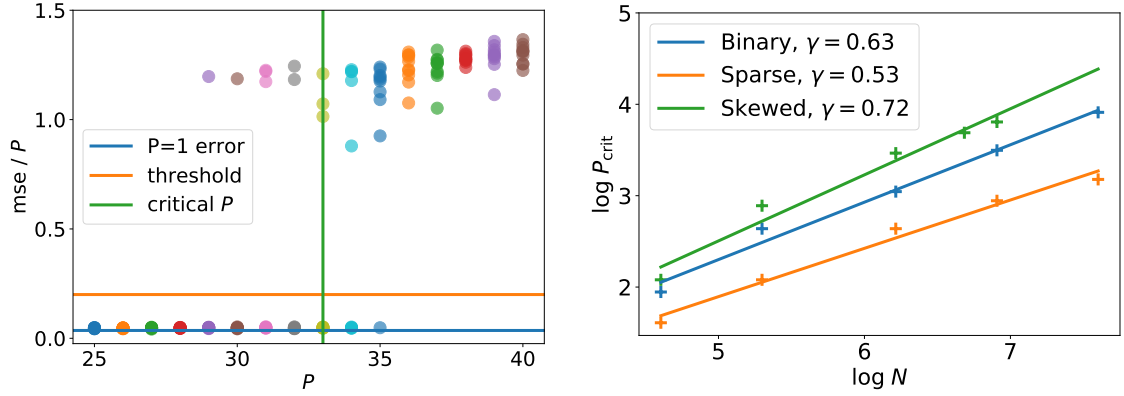


Figure 6: **Scaling of the critical number of patterns that can reliably be reconstructed with mean-field message passing.** (Left) For binary patterns, we plot the final reconstruction error of twenty instances of the mean-field message-passing algorithm as a function of the number of stimuli stored P . We define the critical number of patterns that can be reconstructed as the largest P at which more than half the runs yield an mse better than a threshold value (here, 20% of the trivial mse, i.e. 0.2). $N = 1000$, $\Delta = 0.2\Delta_C$, $\tau = 0$. (Right) We plot the highest number of patterns P_{\max} that could be reconstructed with an error below 20% of the trivial error in at least 50% of cases. For all three models considered, we show experimental results (crosses) and the exponent of a power law fit $P_{\max} \sim N^\gamma$. In all cases, $\tau = 0$ and the noise level Δ was 20% of the critical noise level Δ_c where reconstruction becomes impossible.

\mathbf{W} is a noise matrix with independent and identically distributed entries. Montanari et al. [58] propose an iterative approach to estimate the noise distribution from the observations \mathbf{Y} . It is an interesting direction for future work to explore both strategies for the problem of reconstructing stimuli considered here.

The relation to other potential methods Another candidate for reconstructing patterns from the connectivities are spectral methods. The most widely used variant of these algorithms is principal component analysis (PCA), whose aim is to discover the directions in the data matrix \mathbf{X} that best explain the variance in the data. These directions are identified as the eigenvectors corresponding to the largest eigenvalues of the empirical covariance $\mathbf{X}^\top \mathbf{X} / P$. The key problem one needs to solve so apply spectral methods to reconstruction problems is how to recover the stimuli from these eigenvectors. Spectral methods have some advantages - they are easy to implement, and non-parametric - but they also have some important disadvantages. Most notably, they do not offer a natural way to incorporate the prior knowledge we have about the structure and distribution of stimuli into the recovery algorithm. The Bayesian framework incorporates this domain knowledge in a transparent way through the generative model of the stored patterns $p_X(\mathbf{x})$.

Reconstructing an extensive number of patterns Another important extension of our work would be the reconstruction of an extensive number of patterns from the connectivity \mathbf{J} , i.e. whether the regime $P \sim \mathcal{O}(N)$ is accessible. This is essentially the problem of factorising a large matrix with extensive rank, which is also known as dictionary learning [59–61]. This is a very hard problem with implications that would go far beyond the application discussed here.

Methods

A formal analogy between problems in inference and statistical physics

It may surprise at first that statistical physics can be helpful in solving and analysing inference problems like the one considered here. The connection between the two becomes more transparent if we introduce the interaction $g(\cdot) \equiv \ln P_{\text{out}}(\cdot)$ to rewrite the posterior as

$$P(\mathbf{X}|\mathbf{J}) = \frac{1}{Z(\mathbf{J})} \prod_i^N P_X(\mathbf{x}_i) \prod_{j>i}^N \exp[g(J_{ij}, W_{ij})]. \quad (31)$$

This distribution describes the posterior density over estimates \mathbf{X} . However, it can also be interpreted as the Gibbs or Boltzmann distribution that describes the properties of complex, disordered systems such as glasses. This analogy can be leveraged by exploiting tools from the statistical physics of disordered systems to tackle the – hard – inference problem that is inferring the patterns from the connectivity \mathbf{J} . The key ideas behind the Low-RAMP algorithm that we discuss throughout this work and AMP algorithms in general first appeared in a paper by Thouless, Anderson and Palmer [62] that dealt with physical systems described by an equilibrium distribution of the type (31). State evolution techniques where first introduced for compressed sensing problems by Donoho, Maleki and Montanari [41] based on ideas from [46], but it too is based on ideas from statistical physics often referred to as the cavity method [47]. For a much more detailed on the links between statistical physics and inference problem, see [40, 49, 63].

Approximate message passing for low-rank matrix reconstruction

We are now in a position to state the Low-RAMP algorithm for the factorisation of symmetric low-rank matrices that in this form was derived by Lesieur [43], building on the previous works deriving AMP-type algorithms for particular instances of this problem class [35, 44, 45]. We refer the interested reader to these papers for details on the derivation of this class of algorithms and their relation to belief propagation and spectral methods.

To describe the algorithm, we first define the Fisher information matrix as a transformation of the data matrix \mathbf{J} given for the inference:

$$S_{ij}(J_{ij}) \equiv \left. \frac{\partial \ln P_{\text{out}}(J_{ij}|w)}{\partial w} \right|_{w=0} \quad (32)$$

For the channel corresponding to the rectified Hopfield model (2), we find

$$S_{ij}(J_{ij}) = \begin{cases} -\frac{2e^{-\tau^2/2\nu^2}}{\sqrt{2\pi}\nu \operatorname{erfc}(-\tau/\sqrt{2\nu})}, & J_{ij} = 0 \\ \frac{J_{ij} + \tau}{\nu^2} & \text{otherwise.} \end{cases} \quad (33)$$

Low-RAMP is an iterative algorithm: at every step t , it computes a new estimate of the mean $\hat{\mathbf{x}}_i^{t+1}$ and the variance σ_i^{t+1} as

$$\hat{\mathbf{x}}_i^{t+1} = f_{\text{in}}(\mathbf{A}_i^t, \mathbf{b}_i^t) \quad (34a)$$

$$\sigma_i^{t+1} = \partial_{\mathbf{b}} f_{\text{in}}(\mathbf{A}_i^t, \mathbf{b}_i^t) \quad (34b)$$

where the threshold function was defined in Eq. (11) and is repeated here for convenience:

$$f_{\text{in}}(\mathbf{A}, \mathbf{b}) = \frac{1}{Z(\mathbf{A}, \mathbf{b})} \sum_{\mathbf{x} \in \mathcal{X}^P} \mathbf{x} p_X(\mathbf{x}) \exp\left(\mathbf{b}\mathbf{x} - \frac{1}{2}\mathbf{x}^\top \mathbf{A}\mathbf{x}\right). \quad (35)$$

There exists a set of parameters $\mathbf{A}_i \in \mathbb{R}^{P \times P}$ and $\mathbf{b}_i \in \mathbb{R}^P$ for every marginal, which in turn are updated as

$$\mathbf{b}_i^t = \frac{1}{\sqrt{N}} \sum_k^N S_{ki} \hat{x}_k^t - \left(\frac{1}{N} \sum_k^N S_{ki}^2 \sigma_k^t \right) \hat{x}_i^{t-1} \quad (36a)$$

$$\mathbf{A}_i^t = \frac{1}{N} \sum_k^N S_{ki}^2 \hat{x}_k^t \hat{x}_k^{t,\top} \quad (36b)$$

To run the algorithm, we perform these steps:

1. Given the matrix \mathbf{J} , compute the Fisher information matrix \mathbf{S} using Eq. (32).
2. For all $i = 1, \dots, N$, initialise the parameters \mathbf{b}_i and \mathbf{A}_i such that all entries are zero. Initialise all estimators \hat{x}_i^t with a random draw from the prior distribution $p_X(\mathbf{x})$ and set \hat{x}_i^{t-1} to all zeros for the first step. (There is no need to initialise σ_i).
3. Compute first the update to \mathbf{A}_i^t and \mathbf{b}_i^t following Eqs. (36b) and (36a), then compute the new means \hat{x}_i^{t+1} and their variance σ_i^{t+1} using Eqs. (34a) and (34b).
4. Repeat Step 3 until the squared difference between all \hat{x}_i^t and \hat{x}_i^{t+1} is smaller than some predefined threshold ϵ .

We also provide an implementation of this algorithm in a [Python package](#) that was the base of all the programs written for this paper.

Acknowledgements

SG, FK and LZ would like to thank the Department of Mathematics at Duke University, Durham NC, USA, for their hospitality during an extended visit.

References

1. White, J. G., Southgate, E., Thomson, J. N. & Brenner, S. The Structure of the Nervous System of the Nematode *Caenorhabditis elegans*. *Philosophical Transactions of the Royal Society B: Biological Sciences* **314**, 1–340 (1986).
2. Ohyama, T. *et al.* A multilevel multimodal circuit enhances action selection in *Drosophila*. *Nature* **520**, 633–639 (2015).
3. Eichler, K. *et al.* The complete connectome of a learning and memory centre in an insect brain. *Nature* **548**, 175–182 (2017).
4. Xu, C. S. *et al.* A Connectome of the Adult *Drosophila* Central Brain. *bioRxiv*. eprint: <https://www.biorxiv.org/content/early/2020/01/21/2020.01.21.911859.full.pdf> (2020).
5. Scheffer, L. K. *et al.* A Connectome and Analysis of the Adult *Drosophila* Central Brain. *bioRxiv*. eprint: <https://www.biorxiv.org/content/early/2020/04/09/2020.04.07.030213.full.pdf> (2020).
6. Wanner, A. A. & Friedrich, R. W. Whitening of odor representations by the wiring diagram of the olfactory bulb. *Nat. Neurosci.* **23**, 433–442 (Mar. 2020).
7. Briggman, K. L., Helmstaedter, M. & Denk, W. Wiring specificity in the direction-selectivity circuit of the retina. *Nature* **471**, 183–188 (2011).

8. Helmstaedter, M. *et al.* Connectomic reconstruction of the inner plexiform layer in the mouse retina. *Nature* **500**, 168–174 (2013).
9. Kim, J. S. *et al.* Space–time wiring specificity supports direction selectivity in the retina. *Nature* **509**, 331–336 (2014).
10. Mishchenko, Y. *et al.* Ultrastructural Analysis of Hippocampal Neuropil from the Connectomics Perspective. *Neuron* **67**, 1009–1020 (2010).
11. Kasthuri, N. *et al.* Saturated reconstruction of a volume of neocortex. *Cell* **162**, 648–661 (2015).
12. Lee, W.-C. A. *et al.* Anatomy and function of an excitatory network in the visual cortex. *Nature* **532**, 370–374 (2016).
13. Motta, A. *et al.* Dense connectomic reconstruction in layer 4 of the somatosensory cortex. *Science*, eaay3134 (2019).
14. Dorkenwald, S. *et al.* Binary and analog variation of synapses between cortical pyramidal neurons. *bioRxiv*. eprint: <https://www.biorxiv.org/content/early/2019/12/31/2019.12.29.890319.full.pdf> (2019).
15. Motta, A., Schurr, M., Staffler, B. & Helmstaedter, M. Big data in nanoscale connectomics, and the greed for training labels. *Current Opinion in Neurobiology* **55**, 180–187 (2019).
16. Litwin-Kumar, A. & Turaga, S. C. Constraining computational models using electron microscopy wiring diagrams. *Current Opinion in Neurobiology* **58**, 94–100 (2019).
17. Brunel, N. Is cortical connectivity optimized for storing information? *Nature Neuroscience* **19**, 749–755 (2016).
18. Hopfield, J. J. Neural networks and physical systems with emergent collective computational abilities. *Proc. Natl. Acad. Sci. U. S. A.* **79**, 2554–2558 (1982).
19. Tsodyks, M. V. & Feigel'man, M. V. The Enhanced Storage Capacity in Neural Networks with Low Activity Level. *Europhys. Lett.* **6**, 101–105 (1988).
20. Amit, D. J. The Hebbian paradigm reintegrated: Local reverberations as internal representations. *Behavioral and Brain Sciences* **18**, 617–626 (1995).
21. Amit, D. J. & Brunel, N. Model of global spontaneous activity and local structured activity during delay periods in the cerebral cortex. *Cerebral cortex (New York, NY: 1991)* **7**, 237–252 (1997).
22. Pereira, U. & Brunel, N. Attractor dynamics in networks with learning rules inferred from in vivo data. *Neuron* **99**, 227–238 (2018).
23. Hebb, D. O. *The organization of behavior: A neuropsychological approach* (John Wiley & Sons, 1949).
24. Amit, D. J., Gutfreund, H. & Sompolinsky, H. Statistical mechanics of neural networks near saturation. *Annals of physics* **173**, 30–67 (1987).
25. Sompolinsky, H. & Kanter, I. Temporal association in asymmetric neural networks. *Physical review letters* **57**, 2861 (1986).
26. Mongillo, G., Rumpel, S. & Loewenstein, Y. Inhibitory connectivity defines the realm of excitatory plasticity. *Nature neuroscience* **21**, 1463–1470 (2018).
27. Grienberger, C., Milstein, A. D., Bittner, K. C., Romani, S. & Magee, J. C. Inhibitory suppression of heterogeneously tuned excitation enhances spatial coding in CA1 place cells. *Nat. Neurosci.* **20**, 417–426 (2017).
28. Lim, S. *et al.* Inferring learning rules from distributions of firing rates in cortical neurons. *Nature neuroscience* **18**, 1804 (2015).

29. Baik, J., Ben Arous, G. & Péché, S. Phase transition of the largest eigenvalue for nonnull complex sample covariance matrices. *Ann. Probab.* **33**, 1643–1697 (2005).

30. Amit, D. J., Gutfreund, H. & Sompolinsky, H. Storing infinite numbers of patterns in a spin-glass model of neural networks. *Phys. Rev. Lett.* **55**, 1530–1533 (1985).

31. Amit, D. J., Gutfreund, H. & Sompolinsky, H. Spin-glass models of neural networks. *Phys. Rev. A* **32**, 1007–1018 (1985).

32. Nishimori, H. *Statistical Physics of Spin Glasses and Information Processing* 1st ed. (Oxford University Press, Oxford, 2001).

33. Wright, J., Ganesh, A., Rao, S., Peng, Y. & Ma, Y. in *Advances in Neural Information Processing Systems 22* (eds Bengio, Y., Schuurmans, D., Lafferty, J. D., Williams, C. K. I. & Culotta, A.) 2080–2088 (Curran Associates, Inc., 2009).

34. Zou, H., Hastie, T. & Tibshirani, R. Sparse Principal Component Analysis. *Journal of Computational and Graphical Statistics* **15**, 265–286 (2006).

35. Deshpande, Y. & Montanari, A. *Information-theoretically optimal sparse PCA* in *2014 IEEE Int. Symp. Inf. Theory* (IEEE, 2014), 2197–2201.

36. Lesieur, T., Krzakala, F. & Zdeborová, L. *Phase transitions in sparse PCA* in *IEEE International Symposium on Information Theory - Proceedings* (2015), 1635–1639.

37. Matsushita, R. & Tanaka, T. *Low-rank matrix reconstruction and clustering via approximate message passing* in *Advances in Neural Information Processing Systems* (2013), 917–925.

38. Fortunato, S. Community detection in graphs. *Physics Reports* **486**, 75–174 (2010).

39. Decelle, A., Krzakala, F., Moore, C. & Zdeborová, L. Inference and Phase Transitions in the Detection of Modules in Sparse Networks. *Physical Review Letters* **107**, 065701 (2011).

40. MacKay, D. J. *Information Theory, Inference and Learning Algorithms* (Cambridge University Press, 2003).

41. Donoho, D. L., Maleki, A. & Montanari, A. Message-passing algorithms for compressed sensing. *Proceedings of the National Academy of Sciences* **106**, 18914–18919 (2009).

42. Pearl, J. Fusion, propagation, and structuring in belief networks. *Artificial Intelligence* **29**, 241–288 (1986).

43. Lesieur, T., Krzakala, F. & Zdeborová, L. Constrained low-rank matrix estimation: phase transitions, approximate message passing and applications. *J. Stat. Mech. Theory Exp.* **2017**, 073403 (2017).

44. Fletcher, A. K. & Rangan, S. Iterative Reconstruction of Rank-One Matrices in Noise. *Inf. Inference A J. IMA*. arXiv: [1202.2759](https://arxiv.org/abs/1202.2759) (2012).

45. Matsushita, R. & Tanaka, T. *Low-rank matrix reconstruction and clustering via approximate message passing* in *Adv. Neural Inf. Process. Syst.* **26** (2013).

46. Bolthausen, E. An Iterative Construction of Solutions of the TAP Equations for the Sherrington–Kirkpatrick Model. *Commun. Math. Phys.* **325**, 333–366 (2014).

47. Mézard, M., Parisi, G. & Virasoro, M. A. SK Model: The Replica Solution without Replicas. *Europhys. Lett.* **1**, 77–82 (1986).

48. Mézard, M., Parisi, G. & Virasoro, M. A. *Spin Glass Theory and Beyond* 317 (1987).

49. Zdeborová, L. & Krzakala, F. Statistical physics of inference: thresholds and algorithms. *Adv. Phys.* **65**, 453–552 (2016).

50. Lesieur, T., Krzakala, F. & Zdeborová, L. *MMSE of probabilistic low-rank matrix estimation: Universality with respect to the output channel* in *2015 53rd Annu. Allert. Conf. Commun. Control. Comput.* (IEEE, 2015), 680–687.

51. Cover, T. M. & Thomas, J. A. *Elements of Information Theory* (John Wiley & Sons, 2006).

52. Bandeira, A. S., Perry, A. & Wein, A. S. Notes on computational-to-statistical gaps: predictions using statistical physics. *arXiv preprint arXiv:1803.11132* (2018).

53. Tsodyks, M. V. Associative Memory in Asymmetric Diluted Network with Low Level of Activity. *Europhys. Lett.* **7**, 203–208 (1988).

54. Barber, D. *Bayesian Reasoning and Machine Learning* 735 (Cambridge University Press, 2012).

55. Manoel, A., Krzakala, F., Tramel, E. W. & Zdeborova, L. *Streaming Bayesian inference: Theoretical limits and mini-batch approximate message-passing* in *2017 55th Annu. Allert. Conf. Commun. Control. Comput.* (IEEE, 2017), 1048–1055. eprint: [1706.00705](https://arxiv.org/abs/1706.00705).

56. Dempster, A. P., Laird, N. M. & Rubin, D. B. Maximum likelihood from incomplete data via the EM algorithm. *Journal of the Royal Statistical Society: Series B (Methodological)* **39**, 1–22 (1977).

57. Krzakala, F., Mézard, M., Saussat, F., Sun, Y. & Zdeborová, L. Probabilistic reconstruction in compressed sensing: algorithms, phase diagrams, and threshold achieving matrices. *Journal of Statistical Mechanics: Theory and Experiment* **2012**, P08009 (2012).

58. Montanari, A., Ruan, F. & Yan, J. Adapting to unknown noise distribution in matrix denoising. *arXiv preprint arXiv:1810.02954* (2018).

59. Mallat, S. G. & Zhang, Z. Matching pursuits with time-frequency dictionaries. *IEEE Transactions on signal processing* **41**, 3397–3415 (1993).

60. Elad, M. & Aharon, M. Image denoising via sparse and redundant representations over learned dictionaries. *IEEE Transactions on Image processing* **15**, 3736–3745 (2006).

61. Mairal, J., Bach, F., Ponce, J. & Sapiro, G. Online learning for matrix factorization and sparse coding. *Journal of Machine Learning Research* **11** (2010).

62. Thouless, D. J., Anderson, P. W. & Palmer, R. G. Solution of 'Solvable model of a spin glass'. *Philosophical Magazine* **35**, 593–601 (1977).

63. Mézard, M. & Montanari, A. *Information, Physics and Computation* (Cambridge University Press, 2009).